CHINA FOUNDRY Research & Development
Vol.16 No.2 March 2019
https://doi.org/10.1007/s41230-019-8080-3

Dendritic branching patterns in platforms of complex Ni-based single crystal castings

Min Huang[1,2], *Gong Zhang[1], Dong Wang[1], Zhi-cheng Ge[1], Yu-zhang Lu[1], Xiang-wei Jiang[1] and Lang-hong Lou[1]

1. Institute of Metal Research, Chinese Academy of Sciences, Shenyang 110016, China

2. University of Chinese Academy of Sciences, Beijing 100049, China

Abstract: Dendritic branching patterns at variable cross-sections in Ni-based single crystal (SX) castings of different generations were investigated using optical microscope (OM), electro probe microanalyzer (EPMA), differential scanning calorimeter (DSC), Thermo-Cal software and Pro-CAST software. Results show that the dendritic branching patterns are similar in outward platform in SXs of different generations. That is, the primary dendrites (PDs) are introduced into the platform by developing a series of secondary dendrites (SDs) to occupy the bottom of the platform, and the ternary dendrites (TDs) originating from these SDs grow upward to fill up the platform. With the SX generation increasing, the undercooling of melts in the inward platform increases significantly due to the increasing alloying elements and the segregation in the directional solidification (DS) process, and the growth velocity of the dendrite tip increases according to the dynamic model of dendrite growth, which is beneficial for the high-order dendrite development. The stronger dendritic branching ability is shown in the inward platform of the higher generation Ni-based SX.

Key words: dendritic branching patterns; platform; undercooling

CLC numbers: TG146.1+5 **Document code:** A **Article ID:** 1672-6421(2019)02-110-08

Due to excellent high temperature performances, Ni-based single crystal (SX) superalloys have been widely used in the aerospace field, especially in manufacturing turbine blades for aero-engines [1]. With the modern engine efficiency improving, the inlet temperature of the turbine increases, and this requires higher temperature capability of SX superalloys [2]. In addition, the alloying elements increase with SXs developing. Consequently, the directional solidification (DS) process is increasingly complicated [3–6], and the elements segregation is more and more serious. Preventing defects, such as stray grains [7–9], misorientation, low angle boundary [10–12] and high angle boundary, for complex alloy systems in the DS process becomes challenging. Therefore, it is necessary to pay attention to the DS process for SX castings of different generations.

Owing to the complex geometry shape and intricate air-cooling channels of turbine blades, asymmetric heat flux and cross-section transients influence the shape of the liquidus isotherm, and consequently, the dendrite growth [13–14]. The dendrite growth is closely connected with the solidification defects, which further affects the performances of SX castings. Thus, it is essential to understand the detailed dendrite development in SX blades. Some researchers [10, 12, 15–18] investigated the dendritic branching patterns at variable cross-sections under different solidification conditions, and it was found that the primary dendrites (PDs) can be introduced into the platforms by developing a series of secondary dendrites (SDs) forward, and the SDs would produce new dendrite branches if the thermal condition was suitable.

In fact, mastering the entire dendrite growth in the DS process can direct the production of SX blades with a complex shape. Also, forming the dendritic branching patterns can be useful for manufacturing the SX castings with a specific direction. Furthermore, studying the dendrite growth in different generations of SXs is beneficial for the acquisition of SX castings with different compositions. Therefore, some experiments should be performed in this field. In this work, the dendritic branching patterns within platforms in SXs of different generations were investigated in detail, and the reasons leading to the different dendritic branching patterns were discussed. These results are expected to

***Gong Zhang**

Male, born in 1978, Senior Engineer. His research interests mainly focus on nickel-base single crystal superalloy.

E-mail: gzhang@imr.ac.cn

Received: 2018-06-22; Accepted: 2018-11-15

direct the industrial production of complex SX components and to increase the yield of SX turbine blades.

1 Experimental

Three different generations of Ni-based SX superalloys with their nominal compositions are shown in Table 1. To investigate the dendritic branching patterns at variable cross-sections in SX castings, a casting model with one body and four platforms was designed. Several size parameters used in the model are labeled in Fig. 1. The platform near the center of the furnace was the inward platform, while the platform furthest from the center of the furnace was the outward platform.

The DS experiment was carried out in a Bridgman high-rate solidification (HRS) industrial vacuum furnace [19]. The same solidification parameters were set for the three SXs during the whole DS process. Temperatures of holding furnace in the upper hot-zone and the lower-zone were set as 1,793 K and 1,823 K,

Table 1: Nominal composition (wt%) of Ni-based single crystal superalloys

Alloy	Cr	Co	Mo	W	Ta	Al	Ti	Re	Ni
D1	12	9	1.9	3.8	5	3.7	4.14	-	Bal.
D2	5	10	2	6	8.7	5.6	-	3	Bal.
D3	3.5	9	1.5	6	8	6	-	4	Bal.

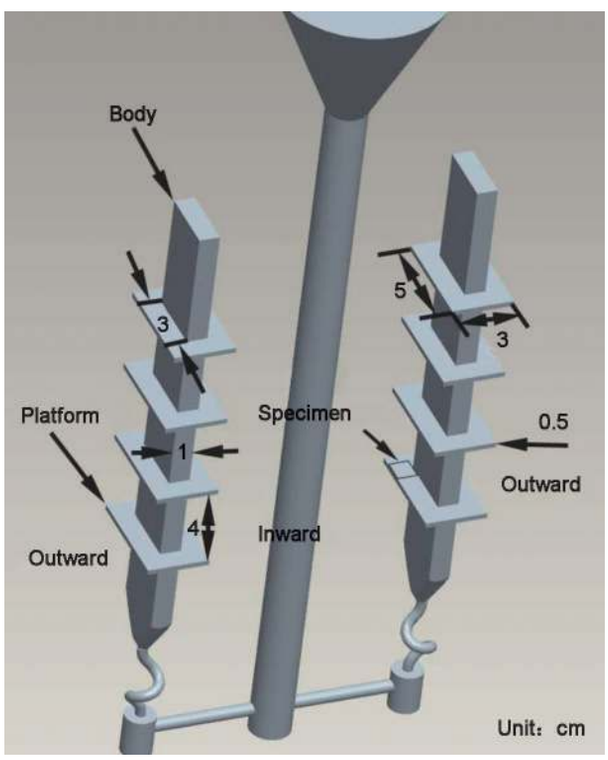

Fig. 1: Schematic diagram and size of castings used in this work

respectively. After the heat preservation for thermal equilibrium, the mold was withdrawn at the rate of 3 mm·min^{-1}. In order to observe dendritic branching patterns, specimens at the same position of four inward platforms were cut by wire electro discharge machining (EDM) as illustrated in Fig. 1. All six surfaces of the specimens were ground, polished, and etched by $CuSO_4$ + HCl + H_2O solution for micro analysis. The arrangement of dendrite array in the six surfaces was observed by optical microscopy (OM), and the results were combined to form the stereoscopic images.

In addition, the specimens in the body were cut for comparison (Fig. 2). The primary dendrite arm spacing (PDAS) of specimens at different positions was calculated according to equation (1):

$$\lambda_1 = (S/N)^{1/2} \quad (1)$$

where λ_1 (μm) is the PDAS, S (μm^2) is the total area of metallographic photo, and N is the number of dendrites in the photo. The eutectic volume fraction in different positions was measured by Image Pro Plus 6.0 software. The element contents in the body and the platform were measured by electro probe microanalyzer (EPMA). The liquidus temperatures of the three SXs were obtained by differential scanning calorimeter (DSC) experiments with the heating rate of 10 K·min^{-1}. The solid-liquid interface temperatures of the three SXs during DS process were calculated by Thermo-Cal software. The distribution of the temperature field was simulated by Pro-CAST software.

2 Results

2.1 Dendritic branching patterns

According to results of the macro analysis, dendritic branching patterns at variable cross-sections in four platforms with different heights are the same in a casting. The platform at the bottom is chosen to demonstrate the dendritic branching growth. Figure 3 shows the dendritic branching patterns in the inward and outward platforms of the three SXs. In the outward platform, the dendritic branching patterns are similar with each other from the first generation SX D1 to the third generation SX D3. At the variable cross-section, a series of secondary dendrites (SDs) develop from the PDs and occupy most of the bottom of the platform. Then, the ternary dendrites (TDs) originating from these SDs grow upward to fill up the platform.

However, the dendritic branching patterns in the inward platforms are different. In the first generation SX D1 and the second generation SX D2, the bottom of the platform is mostly occupied by the SDs. In addition, there are also some TDs in the corner of the bottom of the platform [Fig. 3(a–b)]. In the third

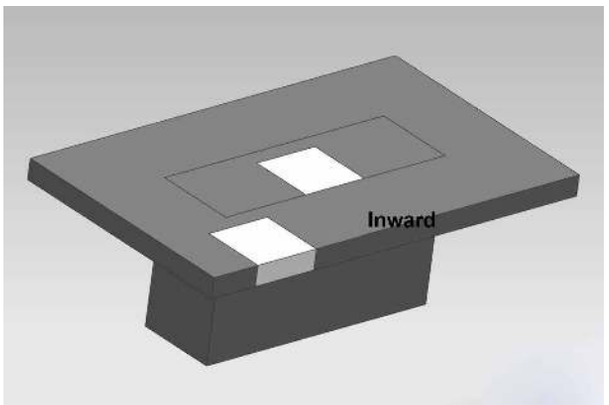

Fig. 2: Schematic diagram of sampling location in complex castings

generation SX D3, there are just several SDs at the bottom, and most of the platform bottom is occupied by the TDs [Fig. 3(c)].

The microstructures of the specimens cut from the inward platform were analyzed to further demonstrate the dendritic branching patterns of the three SXs. In SX D1 as illustrated in Fig. 4(a), the dendrites at the bottom of the platform mainly develop in the form of SDs. Subsequently, TDs developed from these SDs fill up the whole platform upward, and many crisscross dendrites are found on the top of the platform, as shown in Fig. 4(b). In the second generation SX D2, TDs originating from the SDs at the bottom appear in the corner of the platform, as illustrated in Fig. 5(a). Then, TDs and quaternary dendrites (QDs) develop from these SDs and TDs at the bottom to fill the platform upward, and the corresponding

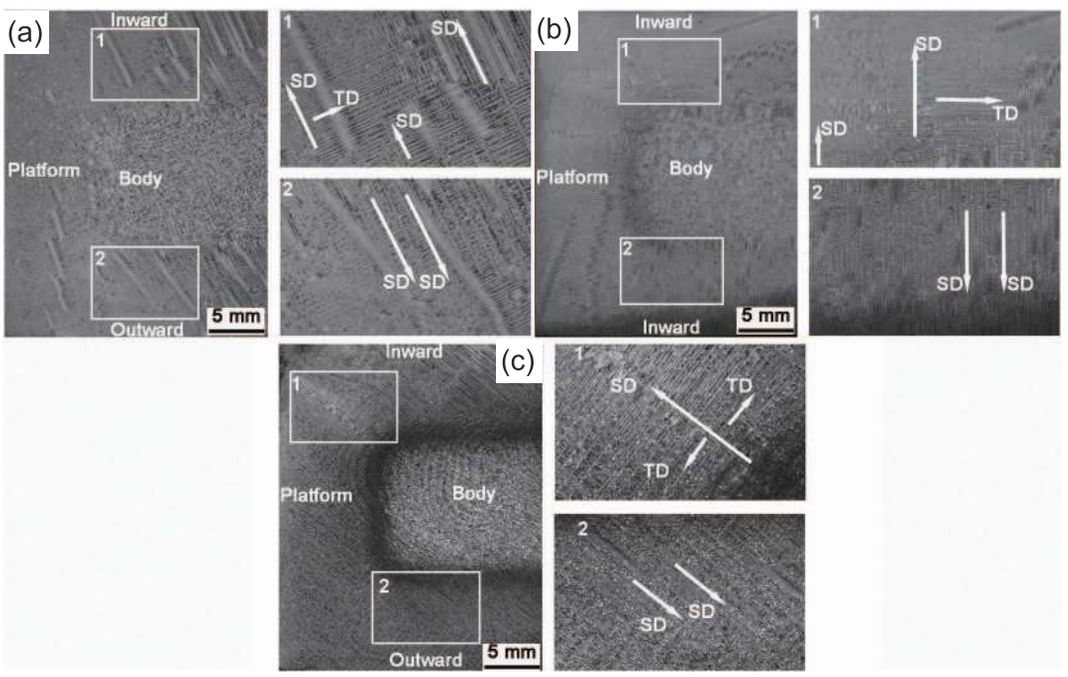

Fig. 3: Dendrite morphology and partial enlarged detail at platform bottom in single crystal castings of different generations: (a) D1, (b) D2, (c) D3

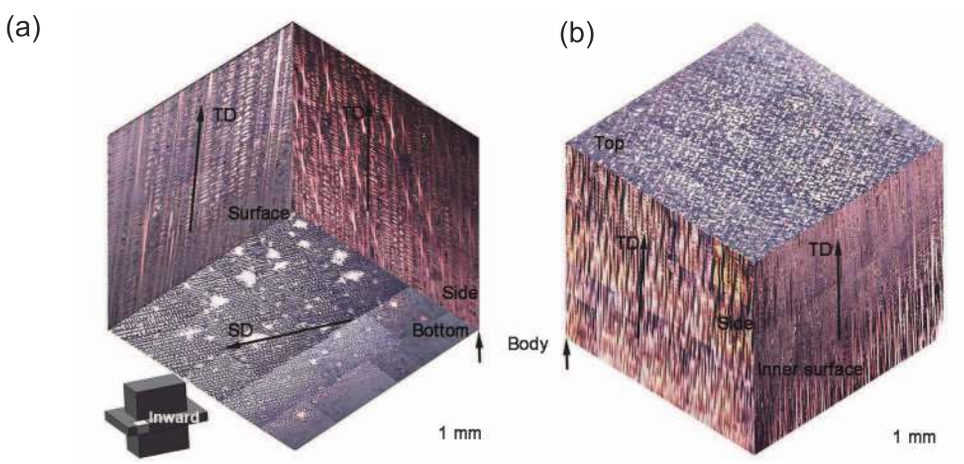

Fig. 4: Dendritic branching patterns in six surfaces in inward platform of D1: (a) view from bottom of casting; (b) view from top of casting

crisscross dendrite morphologies are shown in Fig. 5(b). However, the whole inward platform is still mostly filled up with TDs upward in the second generation SX D2. In the third generation SX D3 as shown in Fig. 6(a), several coarse SDs occur at the bottom, and TDs originating from these SDs occupy most of the bottom of the platform to restrict the growth of other SDs. Then, QDs develop from these TDs to fill up the platform upward, which is consistent with the crisscross dendrites in Fig. 6(b).

2.2 Solidification characteristic parameters

The PDAS and eutectic volume fraction in the body and platform at the same height were measured. As shown in Fig. 7(a), the PDAS gradually decreases both in the body and platform with the SX generation increasing, and the PDAS in the platform is smaller than that in the body in the same generation. As shown in Fig. 7(b), the eutectic volume fraction increases both in the body and the platform with the SX generation increasing, and the eutectic volume fraction in the platform is greater than that in the body in the same generation. EPMA was used to measure the micro-area composition in the body and the platform, and the segregation coefficients were calculated as shown in Table 2. It is found that the elements Ti and Ta with low melting points tend to segregate to the interdendritic region, while the elements with high melting points such as Re and W tend to segregate to the dendrite core. The segregation of the elements in the platform is more serious than that in the body.

2.3 Distribution of temperature field

Due to the same solidification parameters used in the DS process of the three SXs, the distributions of temperature field in the platform are similar with each other as shown in Fig. 8. It is found that the temperature of melts in the corner of the inward platform firstly decreases to the solidus temperature, which causes the melts in the inward platform to always be in an undercooled condition. Therefore, the temperature in the inward platform is lower than that in the outward platform.

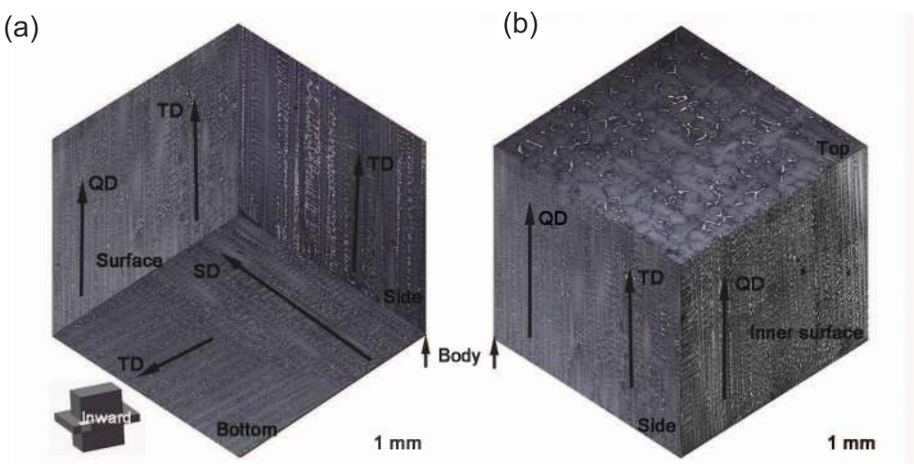

Fig. 5: Dendritic branching patterns in six surfaces in inward platform of D2: (a) view from bottom of casting; (b) view from top of casting

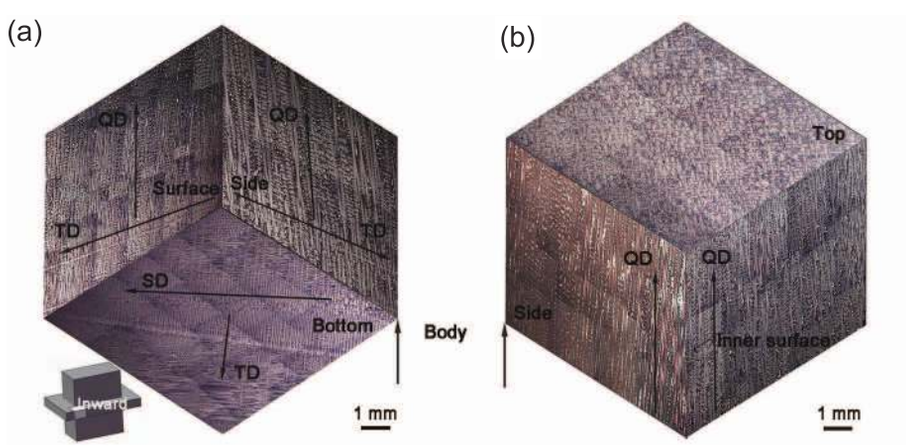

Fig. 6: Dendritic branching patterns in six surfaces in inward platform of D3: (a) view from bottom of casting; (b) view from top of casting

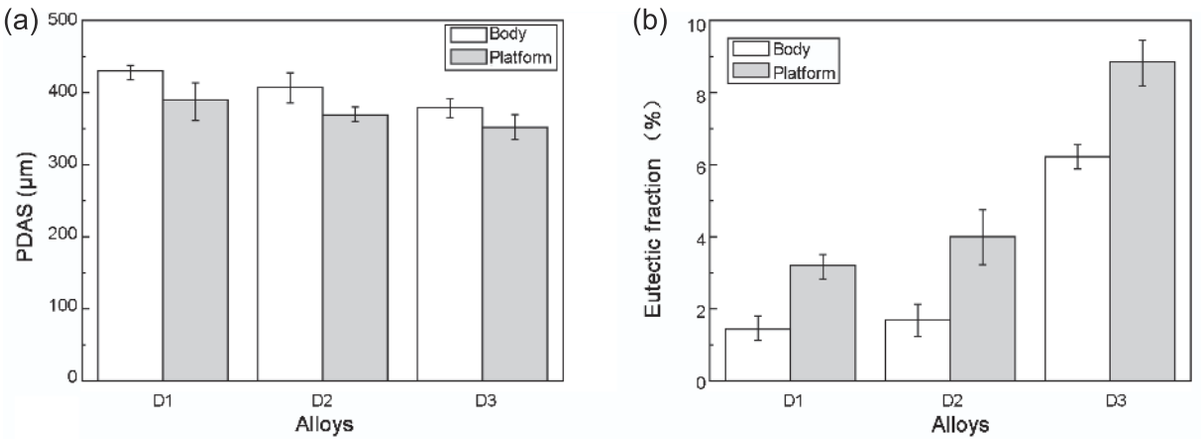

Fig. 7: Solidification characteristic parameters for different generations of Ni-based single crystals: primary dendrite arm spacing (a) and eutectic volume fraction (b) both in body and platform

Table 2: Distribution of elements in dendrite core and interdendritic region and segregation ratio in Ni-based single crystal superalloys

Alloy	Position		Cr	Co	Mo	W	Ta	Al	Ti	Re
D1	Body	Dendrite core	13.08	10.39	1.56	4.50	2.85	3.49	2.62	-
		Interdendritic	12.44	9.10	1.82	2.41	4.32	3.71	5.05	-
		Segregation ratio	1.05	1.14	0.86	1.87	0.66	0.94	0.52	-
	Platform	Dendrite core	13.02	10.45	1.58	4.11	2.64	3.53	2.91	-
		Interdendritic	8.12	7.99	1.07	1.26	4.95	2.24	7.50	-
		Segregation ratio	1.60	1.31	1.48	3.26	0.53	1.58	0.39	-
D2	Body	Dendrite core	4.60	11.07	1.50	6.84	5.08	5.20	-	3.04
		Interdendritic	4.86	10.26	1.72	4.72	7.72	5.84	-	1.81
		Segregation ratio	0.95	1.08	0.87	1.45	0.66	0.89	-	1.68
	Platform	Dendrite core	4.75	11.49	1.61	9.06	2.94	4.94	-	4.04
		Interdendritic	5.85	12.13	2.00	5.63	5.65	6.75	-	1.79
		Segregation ratio	0.81	0.95	0.81	1.61	0.52	0.73	-	2.26
D3	Body	Dendrite core	3.63	10.36	1.35	7.68	5.19	5.25	-	3.94
		Interdendritic	2.90	8.47	1.22	4.08	9.79	6.74	-	1.54
		Segregation ratio	1.25	1.22	1.10	1.88	0.53	0.78	-	2.56
	Platform	Dendrite core	3.50	10.04	1.38	7.78	4.95	5.33	-	3.83
		Interdendritic	3.09	8.38	1.21	3.31	9.81	7.02	-	0.90
		Segregation ratio	1.13	1.20	1.14	2.35	0.50	0.76	-	4.26

2.4 Characteristic temperatures

In the DS process of Ni-based SX superalloys, the castings solidified with the dendrites putting forward at the solid-liquid interface. Due to the different melting points of elements, the dendrite core was formed at first containing more elements with a high melting point, while the elements with a low melting point were expelled to the front of the solid-liquid interface, and finally solidified to form an interdendritic region [20–21]. Therefore, the temperature at the solid-liquid interface could be approximately equal to the melting point of the interdendritic composition. Based on the interdendritic composition of the platform as shown in Table 2, the interface temperatures (marked as T^*) of the three SXs were calculated by Thermo-Cal software and the results are listed in Table 3. In addition, the liquidus

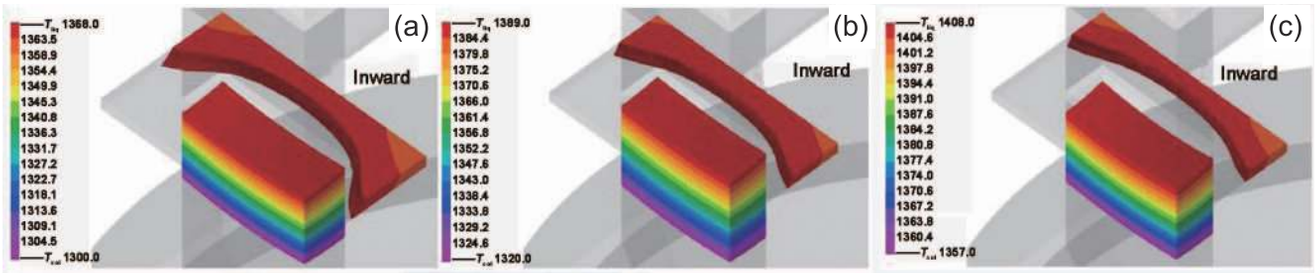

Fig. 8: Distribution of temperature field in platform in directional solidification process: (a) D1; (b) D2; (c) D3

temperatures of the three SXs measured by DSC experiments are shown in Fig. 9. It is seen that both the solidus temperatures and the liquidus temperatures increase with the SX generation increasing.

Table 3: Characteristic temperatures, undercooling and dendritic growth velocity in Ni-based single crystal superalloys.

Alloy	DSC T_L (°C)	Thermo-Cal T^* (°C)	Undercooling ΔT (K)	Velocity (m·s^{-1})
D1	1,345	1,328	17	0.0052
D2	1,411	1,378	33	0.037
D3	1,416	1,374	42	0.0759

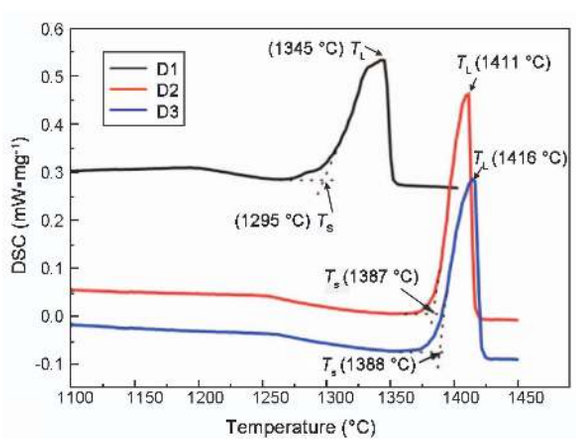

Fig. 9: DSC curves of three Ni-based single crystals with different generations

3 Discussion

The dendritic branching patterns at variable cross-sections of castings in the DS process are influenced by both the temperature field [16] and the alloy composition [22].

3.1 Effect of temperature field

In this work, the same solidification condition was set during the DS process in the three SXs, and the distributions of the temperature field in the three SXs are similar with each other (Fig. 8). However, there are several differences at different positions of the platform. Compared with the outward platform, the inward platform is far away from the heating elements of the furnace as illustrated in Fig. 1. Therefore, the temperature in the inward platform is lower than that in the outward platform, which is consistent with the simulation results. During the DS process, the temperature of the liquid metal in the corners of inward platform firstly decreases to the solidus temperature, keeping the melts here in a larger undercooling. However, even in the corner of inward platform, the undercooling still does not exceed the critical nucleation undercooling, and no stray grains appear, as shown in Fig. 3. Therefore, there is enough time and space for the PDs in the body to be introduced into the platform by developing high order dendrites [7, 23], and the complex dendritic branching patterns are presented [24]. However, due to the smaller undercooling in the outward platform of the three SXs, similar dendritic branching patterns with a series of TDs appear upright as shown in Fig. 3.

3.2 Effect of alloy composition

It is known that the driving force of dendrite growth is undercooling in front of the dendrite tip. According to the following relationship, the undercooling usually consists of four parts:

$$\Delta T=\Delta T_r+\Delta T_T+\Delta T_C+\Delta T_k \quad (2)$$

where ΔT_r (K) is the curvature undercooling, ΔT_T (K) is the thermal undercooling, ΔT_C(K) is the constitutional undercooling, and ΔT_k (K) is the kinetic undercooling. In the case of the conventional castings, the influence of curvature and attachment kinetics on undercooling can be ignored [25]. As for the directional growth of alloys, especially for the directional solidification, the latent heat is transmitted out from the solidified solid phase when imposing the positive temperature gradient, and the solute will be expelled to the front of dendrite tip. In the situation of the first approximation, the effect of latent heat on dendrite growth is ignored [25], and only the diffusion of the solute is the limiting factor. Therefore, the thermal undercooling is ignored, and only the constitutional undercooling is considered as shown in equation (3):

$$\Delta T\approx\Delta T_C \quad (3)$$

Many research [26–28] has been carried out to calculate the constitutional undercooling. Here, the undercooling ΔT_c is calculated according to its definition as shown in equation (4):

$$\Delta T_C=T_L-T^* \quad (4)$$

where T_L is the liquidus temperature of alloy melts in theory, and T^* is the temperature at the solid-liquid interface during

the DS process. With the SX generation increasing, the levels of refractory elements (Re, W, Ta) increases, and therefore the liquidus temperature increases (Fig. 9). In addition, the temperature at the solid-liquid interface is associated with the alloy composition in the interdendritic region, which is connected with the element segregation. Though there are many elements in the SX superalloy, the effect of Re on the segregation is the greatest [29]. Therefore, the temperature at the solid-liquid interface is mainly affected by Re. To sum up, the constitutional undercooling is mostly influenced by Re according to equation (4), which is consistent with previous studies [26]. In fact, in Ni-based SX superalloy, Re is usually used to distinguish the SX generation. In this work, there is a great difference of alloy compositions in SX of different generations. Substituting the variation of alloy compositions with the variation of SX generation in the following discussion is more reasonable to some extent.

As shown in Fig. 7, the PDAS decreases and the eutectic volume fraction increases with the SX generation increasing both in the body and in the platform. The PDAS is inversely proportional to the temperature gradient G and the solidification rate V [30], which are both related to the undercooling of the melts. The eutectic phases containing many γ' forming elements were produced in the final solidification stage. The greater the eutectic volume fraction, the greater the difference between the solidified and the unsolidified regions. Therefore, the element segregation is more serious, which further influences the undercooling in front of the solidification. The effect of undercooling on dendritic branching patterns in the inward platform will be discussed in detail in the following.

As shown in Table 3, with the SX generation increasing, the undercoolings in the inward platform of the three SXs are 17, 33 and 42 K, respectively. That is, the undercooling increases with the SX generation increasing. According to the dynamic model of dendrite growth, also named Kurz-Giovanola-Trivedi (KGT) model, the relationship between the growth velocity of the dendrite tip and the undercooling can be defined as shown in equation (5) [31]:

$$v(\Delta T)=a_2\cdot(\Delta T)^2+a_3\cdot(\Delta T)^3 \quad (5)$$

where a_2 and a_3 are coefficients of dendrite growth, and their orders of magnitude are both 10^{-6} [31]. The growth velocity of dendrite tip in the three SXs is calculated as shown in Table 3. It is found that, with SX generation increasing, the growth velocity of dendrite tip increases significantly. Once the growth velocity exceeds the critical velocity, the corresponding dendritic branching ability is enhanced, which is beneficial for the development of high order dendrites. In this situation, the inward platform is filled up with higher-order dendrites in D3, and different dendritic branching patterns are shown in SXs of different generations in Fig. 3.

In the end, the different dendritic branching patterns in the platform can be summarized as follows. As illustrated in Fig. 10 (a1)–(a2), when meeting with the platform, the SDs originate from the PDs in the body, occupying the bottom of the platform. Afterwards, a series of TDs branching from these SDs grow upright to fill the platform, which is the basic dendritic branching patterns in Ni-based SXs, named Pattern One. In this work, Pattern One is the dendritic branching pattern observed in the outward platforms of D1, D2 and D3. Another case is illustrated in Fig. 10 (b1)–(b2). The TDs will further branch from the SDs at the bottom, and most of the bottom in the platform is occupied by these TDs. Afterwards, new higher-

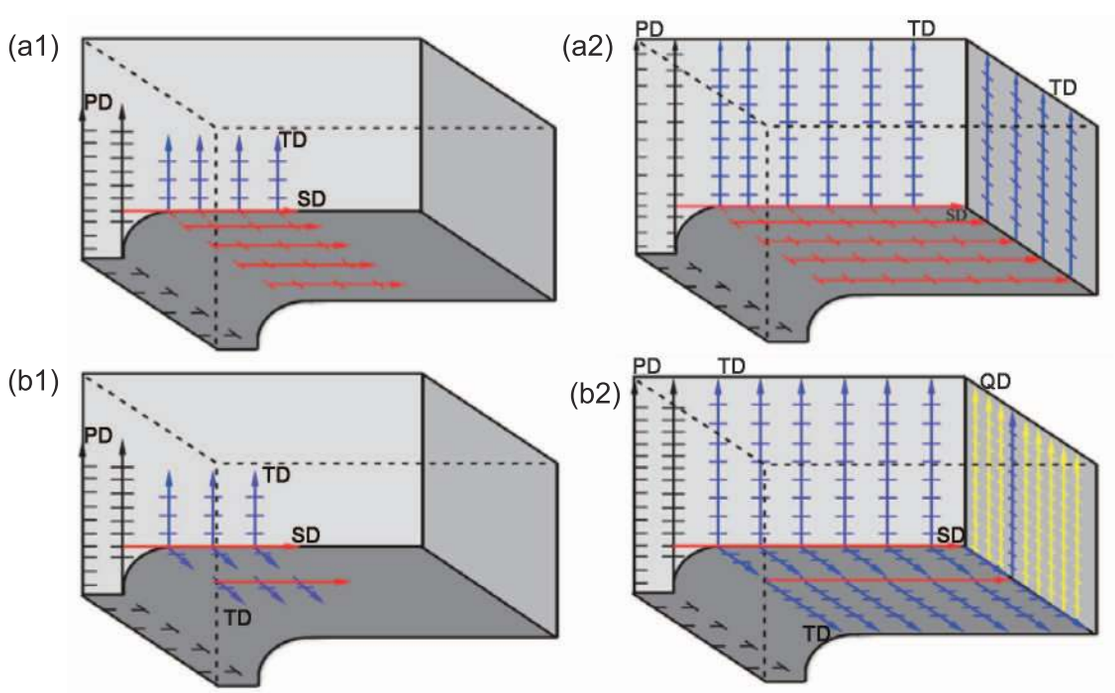

Fig. 10: Schematic diagram of different dendritic branching patterns in platforms: (a1–a2) Pattern One (b1–b2) Pattern Two

order dendrites developing from the TDs grow upright to fill the platform, which tends to occur in the higher generation SXs, named Pattern Two. This is the phenomenon observed in the inward platform of D3.

4 Conclusions

In this work, the dendritic branching patterns at variable cross-sections of three different generations of Ni-based SX superalloys: D1, D2, and D3, were investigated. According to the results, the following conclusions can be drawn:

(1) In the outward platform, the undercooling is smaller. The dendritic branching patterns are similar with each other from the first generation SX D1 to the third generation SX D3. The PDs are introduced into the platform by developing a series of SDs to occupy most of the bottom of the platform, and TDs originating from these SDs grow upward to fill up the platform.

(2) In the inward platform, the undercooling is greater. Due to the high levels of alloying elements and the serious segregation of compositions during DS process, the undercooling of melts increases with SX generation increasing, which leads to the significant increase of the growth velocity of dendrite tip, and the ability of dendrite branching is enhanced, which is beneficial for high order dendrite development. Consequently, in the third generation SX D3, the platform is filled up with the higher-order dendrites upward.

References

[1] Sun X F, Jin T, Zhou Y Z, et al. Research progress of nickel-base single crystal superalloys. Materials China, 2012, 31(12): 1–11. (In Chinese)
[2] Konter M, Thumann M. Materials and manufacturing of advanced industrial gas turbine components. Journal of Materials Processing Technology, 2001, 117: 386–390.
[3] Pollock T M, Murphy W H. The breakdown of single-crystal solidification in high refractory nickel-base alloys. Metallurgical and Materials Transactions A, 1996, 27: 1081–1094.
[4] Meyer ter Vehn M, Dedecke D, Paul U, et al. Undercooling related casting defects in single crystal turbine blades. Superalloys, 1996: 471–479.
[5] Madison J, Spowart J E , Rowenhorst D J, et al. Fluid flow and defect formation in the three-dimensional dendritic structure of nickel-based single crystals. Metallurgical and Materials Transactions A, 2012, 43: 369–380.
[6] Pollock T M, Murphy W H, Goldman E H, et al. Grain defect formation during directional solidification of nickel base single crystals. Superalloys, 1992: 125–134.
[7] Li Y F, Liu L, Huang T W, et al. The formation mechanism, influencing factors and processing control of stray grains in nickel-based single crystal superalloys. Superalloys, 2016: 293–301.
[8] Yang X L, Dong H B, Wang W, et al. Microscale simulation of stray grain formation in investment cast turbine blades. Materials Science & Engineering A, 2004, 386: 129–139.
[9] Meng X B, Li J G, Zhu S Z, et al. Method of stray grain inhibition in the platforms with different dimensions during directional solidification of a Ni-base superalloy. Metallurgical and Materials Transactions A, 2014, 45: 1230–1237.
[10] Napolitano R E, Schaefer R J. The convergence-fault mechanism for low-angle boundary formation in single-crystal castings. Journal of Materials Science, 2000, 35:1641–1659.
[11] Newell M, D'Souza N, Green N R. Formation of low angle boundaries in Ni-based superalloys. International Journal of Cast Metals Research, 2009, 22: 66–69.
[12] D'Souza N, Newell M, Devendra K, et al. Formation of low angle boundaries in Ni-based superalloys. Materials Science & Engineering A, 2005, 413-414: 567–570.
[13] Paul U, Sahm P R, Goldschmidt D. Inhomogeneities in single crystal components. Materials Science & Engineering A, 1993, 173: 49–54.
[14] Elliott A J, Karney G B, Gigliotti M F X, et al. Issues in processing by the liquid-Sn assisted directional solidification technique. Superalloys, 2004: 421–430.
[15] Miller J D, Pollock T M. Stability of dendrite growth during directional solidification in the presence of a non-axial thermal field. Acta Materialia, 2014, 78: 23–36.
[16] Szeliga D, Kubiak K, Sieniawski J. Control of liquidus isotherm shape during solidification of Ni-based superalloy of single crystal platforms. Journal of Materials Processing Technology, 2016, 234: 18–26.
[17] Newell M, Devendra K, Jennings P A, et al. Role of dendrite branching and growth kinetics in the formation of low angle boundaries in Ni-base superalloys. Materials Science & Engineering A, 2005, 412: 307–315.
[18] Zhang X L, Zhou Y Z, Han Y Y, et al. Dendritic growth pattern and dendritic network distortion in the platform of a Ni-based superalloy. Journal of Materials Science & Technology, 2014, 30(3): 223–228.
[19] Huang M, Zhang G, Wang D, et al. Microstructure and stress-rupture property of large-scale complex nickel-based single crystal casting. Acta Metallurgica Sinica (English Letters), 2018, 31(8): 887–896.
[20] Alexandru Paraschiv, Gheorghe Matache, Cristian Puscasu. The effect of heat treatment on the homogenization of CMSX-4 Single-Crystal Ni-based Superalloy. Transportation Research Procedia, 2018, 29: 303–311.
[21] Seo S M, Lee J H, Yoo Y S, et al. A comparative study of the γ/γ' eutectic evolution during the solidification of Ni-base superalloys. Metallurgical and Materials Transactions A, 2011, 42: 3150–3159.
[22] Ma D X, Wu Q, Andreas Buhrig-Polaczek. Undercoolability of superalloys and solidification defects in single crystal components. Advanced Materials Research, 2011, 278: 417–422.
[23] Jia Y L, He L L, Zhao Y S, et al. Determination of undercooling time for stray grain formation of DD11 single crystal superalloy. Journal of Aeronautical Materials, 2015, 35: 8–15. (In Chinese)
[24] Wang W, A. Kermanpur, P.D. Lee, et al. Simulation of dendritic growth in the platform region of single crystal superalloy turbine blades. Journal of Materials Science, 2003, 38: 4385–4391.
[25] Kurz W, Fisher D J, Fundamentals of solidification, 1986
[26] Bogner S, Ivanova E, Muller M, et al. Investigation of the undercoolability of Ni-based alloys using high temperature thermal analysis. Metals, 2015, 5: 1971–1983.
[27] Schempp P, Cross C E, Pittner A, et al. Influence of solute content and solidification parameters on grain refinement of aluminum weld metal. Metallurgical and Materials Transactions A, 2013, 44: 3198–3210.
[28] Chen Z W, He Z, Jie W Q, et al. Growth restriction effects during solidification of aluminium alloys. Transactions of Nonferrous Metals Society of China, 2009, 19: 410–413.
[29] Kearsey R M. Compositional effects on microsegregation behavior in single crystal superalloy systems. Thesis. Carleton University. 2004.
[30] Vijayakumar M, Tewari S N, James E L, et al. Dendrite spacings in directionally solidified superalloy PWA-1480. Materials Science & Engineering A, 1991, 132: 195–201.
[31] Song Y D, Hao H, Gu S W, et al. Research on the effect of dendrite tip growth velocity on the microstructure simulation determination of the approximation of Ivantsov function. Foundry Technology, 2011, 32: 34–38. (In Chinese)

This work was financially supported by the National Key Research and Development Program of China (No. 2017YFB0702904) and the National Natural Science Foundation of China (No. 51631008).